HHS Public Access

Author manuscript

Pain. Author manuscript; available in PMC 2018 December 01.

Published in final edited form as:

Pain. 2017 December ; 158(12): 2461–2474. doi:10.1097/j.pain.0000000000001057.

miRNA-mediated downregulation of KCC2 and VGAT expression in spinal cord contributes to neonatal cystitis-induced visceral pain in rats

Jian Zhang[a], **James Yu**[a], **Pradeep Kannampalli**[a], **Linghui Nie**[b], **Hui Meng**[c], **Bidyut Medda**[a], **Reza Shaker**[a], **Jyoti N. Sengupta**[a], and **Banani Banerjee**[a,*]

[a]Division of Gastroenterology and Hepatology, Department of Medicine, Medical College of Wisconsin, Milwaukee, Wisconsin

[b]Department of Surgery, Medical College of Wisconsin, Milwaukee, Wisconsin

[c]Department of Pathology, Medical College of Wisconsin, Milwaukee, Wisconsin

1. Introduction

The neonatal period is a critical time for the development of the nociceptive neural pathways. Any alteration in the level of neuronal activity during this time may affect normal development. The intrinsic mechanism of early-life noxious stimuli-induced permanent alteration in nociceptive processing is not fully understood. It has been proposed that midbrain (RVM) descending inhibitory and facilitatory systems, which are involved in modulating pain behavior, are possibly affected, [26]. Impairment of the opioid inhibitory pathway has been implicated in the development of painful bladder disorders in animals that have experienced bladder inflammation early in life [6]. In conjunction with these findings, we have recently reported a long-term visceral hyperalgesia and overexpression of spinal NMDA receptor subunit NR1 in adult rats following neonatally-induced cystitis [17]. We have also documented that miRNA-mediated post-transcriptional dysregulation of $GABA_{A\text{-}\alpha 1}$ receptor subunit expression in the lumbosacral (LS) spinal cord could play a role in the pathophysiology of cystitis-induced visceral pain [35].

The γ-aminobutyric acid (GABA) plays a major role in pain modulation in the spinal cord and its function is critically dependent on the activity of intracellular Cl^- regulatory proteins, like the inwardly directed NKCC1 and outwardly directed KCC2 [7; 25; 32]. Under normal conditions, KCC2 is essential for the maintenance of low intracellular Cl^- concentrations in mature neurons and the hyperpolarizing function of GABA in the spinal cord [5; 27]. In certain pathological conditions, such as in diabetic neuropathy, KCC2 is down-regulated or becomes non-functional leading to high intracellular loading of Cl^-. In such conditions, the opening of $GABA_A$ receptor channels results in a rapid efflux of Cl^- due to the reversed

*Corresponding author: Banani Banerjee, MSc., PhD., Associate Professor of Medicine, Division of Gastroenterology, Medical College of Wisconsin, Milwaukee, WI 53226, Tel: 414-456-4493, Fax: 414-456-6361, banerjee@mcw.edu.

The authors declared no competing financial interests.

concentration gradient, which results in depolarization and neuron hyper-excitation [9; 20; 21].

Unlike in adult pain models, where the loss of GABAergic function is observed to be transient, the neonatal cystitis-induced rats, have shown a long-lasting visceral hyperalgesia and down-regulation of spinal $GABA_A$ receptor expression when tested at adulthood [35]. This finding indicates that following early-in-life insults, there could be a permanent impairment of developing GABAergic neurotransmission which might contribute towards its disinhibition and development of chronic pelvic pain (CPP) later in life.

Involvement of miRNAs in chronic visceral pain, including bladder pain syndrome (BPS) and irritable bowel syndrome (IBS) have recently been reported [4; 18; 31; 42]. We have previously demonstrated upregulations of several spinal miRNAs including miR-92b in rats treated with zymosan early-in-life [35]. Interestingly, miR-92b target gene prediction suggests several GABA-associated genes including KCC2 and VGAT. These findings encouraged us to investigate the involvement of miR-92b-mediated post-transcriptional dysregulation of spinal GABAergic transmission in the pathophysiology of zymosan-induced cystitis and chronic pelvic pain. Therefore, in the present study, we intended to examine whether 1) intravesicle zymosan treatment both at neonatal and adult stages affect the expression of miR-92b and its target genes, KCC2 and VGAT, in lumbosacral spinal dorsal horn neurons and 2) miR-92b-mediated post-transcriptional deregulation of GABAergic transmission is the underlying mechanism for the development and maintenance of long-term visceral hyperalgesia following early-in-life-induced cystitis in rats.

2. Materials and Methods

2.1 Animals

Female Sprague Dawley (SD) rats weighing 200 to 250 g were used for this study. For neonatal treatment, time-pregnant rats were purchased from Taconic Farms (Cambridge City, IN) and maintained in separate cages. All animals were housed under controlled conditions with a 12h light-dark cycle and had free access to food and water. The pups were kept with their mother until weaning occurred on P21. The experiments were performed according to the approved guidelines by the Institutional Animal Care and Use Committee at the Medical College of Wisconsin (AUA355) and followed the humane pain management recommendation of the International Association for the Study of Pain (IASP).

2.2 Zymosan-induced cystitis in neonate and adult rats

Three different zymosan treatment protocols were used in this study (Fig. 1A). In protocol 1 (neonatal treatment), two groups of female pups, experimental and control groups, received transurethral zymosan (1% in saline, 100μl) and saline (100μl) respectively from postnatal (P) days 14–16. In protocol 2 (neonatal treatment and adult re-challenge), rats received neonatal zymosan treatment as mentioned in protocol 1 followed by adult zymosan- or saline- re-challenge in adulthood from P57–59. In protocol 3 (adult treatment), rats in experimental and control groups received only zymosan and saline respectively from P57–

59. In all three protocols, rats were euthanized on postnatal day 60 and tissues were obtained for analysis.

2.3 Bladder histology

The extent of bladder damage following zymosan treatment in each protocol was assessed by Hematoxylin and Eosin staining. Histological examination was carried out by a pathologist blinded to the groups and treatment protocols. Different degrees of epithelial loss (e.g., splitting, erosion, and ulceration), reactive epithelial changes (e.g., basal hyperplasia, edema, congestion, bleeding, and vessel's lesions) and inflammation (polymorphonuclear leukocytes, lymphocytes) among the groups were scored. The histological scoring was undertaken based on the following 3 criteria: staining with no inflammatory cell infiltration and minimal erosion and ulceration was scored as (−); staining pattern with a very few inflammatory cell infiltration and low level of edema and vascular congestion was scored as (+); significant infiltration, vascular congestion and erosion was scored as (++/+++). In order to provide numerical scorings for the histological evaluation, the grading (−) was assigned numerical value of 0, grading (+) with value of 1 and gradings (++) & (+++) of values 2 & 3 respectively. The histological scorings between the groups were compared using student t test and presented as mean±SD and values with $p<0.05$ were considered to be significant.

2.4 Total RNA extraction and Qiagen miRNA PCR Array

Total RNA from the dorsal region of the spinal cord (L6-S1) of each rat was isolated using Trizol (Thermo Fisher Scientific, Waltham, MA) according to the manufacturers' instructions. RNA concentration was measured with NanoDrop (Thermo Fisher Scientific). Total RNA was reversely transcribed using miScript II RT Kit (Qiagen, Valencia, CA). The cDNA obtained was used as the template in miScript PreAMP PCR Kit with miScript PreAMP pathway primer mixture (MBRN-120Z, Qiagen). Five pre-Amp samples within each group were pooled to use for miRNA PCR Array. We used the Rat Pain miScript miRNA PCR Array (Neuropathic & Inflammatory miScript miRNAs PCR Array, MIRN-120Z, Qiagen) representing 84 miRNAs known to be involved in the transduction, maintenance, and modulation of pain responses for analyzing miRNA expression profiles in the spinal dorsal horn samples. These miRNAs were selected based on the existing literature reporting their differential expressions in various rodent models of neuropathic and inflammatory pain. The PCR Array reactions were prepared based on the Qiagen protocol using QuantiTect SYBR Green PCR Master Mix (Qiagen). A set of controls were incorporated in each array for proper data analysis using the $\Delta\Delta C_T$ method of relative quantification and for the assessment of reverse transcription and PCR performance. Values of cycle threshold (C_T) obtained for individual miRNAs in the array were uploaded to the Qiagen website for the calculation of fold changes in neonatal cystitis samples compared to saline controls. SNORD-95 was chosen from the group of five housekeeping genes as the best and least varying reference gene.

2.5 Validation of miRNA PCR array results by real-time quantitative RT-PCR

Real-time quantitative RT-PCR was performed to validate the miRNA PCR array results. Total RNA from individual spinal dorsal horn tissues (500 ng) were reverse transcribed using RT^2-first strand kit from Qiagen. The real-time PCR was carried out using the RT^2-

PCR Primer Assay kit and RT^2-SYBR Green master mixes from Qiagen. Individual cDNA preparations (n=5–6/group) were used and results were expressed as relative miRNA expression in terms of C_T values in relation to the amount of reference miRNA expression using formula = $2^{-(C_T\text{miRNA} - C_T\text{SNORD-95})}$.

2.6 Identification and classification of miRNA targets

Predicted miRNA targets were identified using the miRNA2 function tool in the miRNA Body Map program which integrates all miRNA targets predicted by TargetScan Human v5.1, MicroCosm Targets v5, miRDB v3, TarBase v.5c, miRecordsv2, DIANA-microT v3.0, RNA22, and PITA v6 [16]. Targets predicted by three algorithms were selected for further study.

2.7 3'UTR gene constructs and luciferase assay

To confirm that the expressions of KCC2 and VGAT genes are regulated by complimentary binding of their 3′-UTRs by miR-92b-3p, we constructed two pEZX-MT06 vectors carrying 3′UTRs of KCC2 (2088 bp) and VGAT (728 bp) respectively fused downstream of firefly luciferase reporter gene hLuc under SV40 promoter (GeneCopoeia, Rockville, MD). pEZX-MT06 carries dual reporters including one for regulatory detection (firefly) and another for the internal control and signal normalization (Renilla). To determine the optimal concentrations of plasmids and oligonucleotides suitable for luciferase assay, HEK293T cells were co-transfected with plasmids (100 nM or 200 nM) along with several concentrations of MIRDIAN miR-92b mimic or MIRIDIAN miRNA mimic negative control ranging from 50 nM to 200 nM (GE Pharmakon, Lafayette, CO). Since the control miRNAs at higher concentrations of 200 nM demonstrated an inhibitory effect on HEK293 cells, we selected a lower concentration of 100 nM for both the plasmids and oligonucleotides for the transfection study. The cell transfection was carried out in serum free medium using 1% lipofectamine 2000 according to the manufacturer's protocol (Thermo Fisher Scientific). Cells were lysed 24h post-transfection and luciferase activity was measured using a Dual Luciferase Reporter Assay kit (Promega, Madison, WI). The change in dual luciferase activity of the transfected cells in the same well was measured using GloMax 20/20 Luminometer (Promega, Madison, WI) and presented as normalized firefly luciferase activity against Renilla activity. Three independent transfection experiments were carried out for miR-92b-3p mimic and control miRNA using construct carrying either KCC2 or VGAT 3'UTR. The results were expressed as percent reduction of luciferase activity in miR-92b-3p transfected cells in relation to 100% activity for cells transfected with only plasmid carrying 3'UTR of either KCC2 or VGAT.

2.8 miR-92b-3p expression in spinal dorsal horn neurons (L6-S1) using *in situ* hybridization (ISH)

All surgical equipment and reagents were made RNAase-free prior to conducting ISH. Rats were deeply anesthetized with pentobarbital sodium (50 mg/kg i.p.) and perfused transcardially with cold (4°C) phosphate buffer solution followed by perfusion with 4% paraformaldehyde in 0.1 M PBS, pH 7.4. The L6-S1 segments of the spinal cords were collected and incubated in 4% paraformaldehyde overnight at 4°C followed by incubation overnight in 20% sucrose made in 0.1 M PBS. The tissues were then embedded in HistoPrep

(Fisher Scientific, Pittsburgh, PA), and serial sections of 30-μm thickness were taken on a cryostat. The spinal cord sections were then subjected to proteinase K digestion (1μg/ml) (Exiqon, Woburn, MA) for 10 min at 37°C, followed by prehybridization in microRNA ISH hybridization buffer (Exiqon) for 2hr at 55°C. The hybridization with miRCURY LNA-double DIG detection probe hsa-miR-92b-3p (Exiqon, 5'-DIG-AGGCCGGG-CGAGTGCAATA-DIG-3') and the negative control (5'DIG-GTGTAA-CACGTCTATA-CGCCCA-DIG-3') was carried out overnight at 55°C. After several washes with prehybridization buffer containing various percentages of SSC and finally with PBST (PBS +0.1% Tween 20), tissues were incubated in ISH blocking buffer (10% sheep serum + PBST) for 2 hr. This step was followed by incubation with anti-digoxigenin-fluorescence (1:500, Roche, Indianapolis, IN) for 2hrs at room temperature.

After final washings, slides were examined under a Nikon Eclipse 50i fluorescent microscope (Nikon Instruments Inc. Melville, NY) using narrow band cubes for Alexa 488 (DM505, excitation filter 470–490, barrier filter 515–550 nm). Images were captured with a Nikon Sight DS-Fi1 high-resolution digital camera and processed using Adobe Photoshop CS6 program. To maintain the consistency of image capturing, we used the same time of exposure, gain, and gamma adjustment for the control and experimental samples. Images were then opened in Image J program (NIH, Bethesda, MD) and the free hand tool was used to trace the outline of each cell. The fluorescence images were converted into grey mode. Arbitrary grey scale units (in the range of 1–255) were assigned to quantify the intensity of staining of a given cell. Non-specific background staining was measured in a similar way by selecting cells with staining below the threshold limit for differentiating positively stained cells. We selected one section per animal from both neonatal zymosan- and saline-treated groups and only cells containing a darker nucleus were selected for analysis. Intensity of staining for 5 to 10 cells per section was measured and average intensity of staining from 3 sections per group was determined. The cell counts were performed by an investigator blinded to the experimental conditions. The mean intensity of staining from zymosan-treated rats was compared that with saline-treated controls using the student t test and presented as mean±SD and values with $p<0.05$ were considered to be significant.

2.9 KCC2 (Slc12a5) and VGAT (Slc31a1) gene expression in spinal dorsal horn neurons (L6-S1) by quantitative RT-PCR

Total RNA was extracted from individual spinal dorsal horn sample (L6-S1) from rats receiving 3 different treatment protocols (fig.1A) using Trizol (Thermo Fisher Scientific). The reverse transcription for individual sample was carried out with iScript cDNA synthesis kit (Bio-Rad, Richmond, CA) in iCycler (Bio-Rad) using 500 ng total RNA from each sample. Real-time PCR was performed using iQ SYBR Green Supermix (Bio-Rad) in a total volume of 25μl of reaction mixture containing 5 picomole forward and reverse primers and 2μl cDNA preparation as the template. The primers used for KCC2 were (sense): 5'-GTTCCCGAAGAGACAGCTTG-3', and (antisense) 5'-GAGCCGCTGACTTATCCTTG-3'. The primers for VGAT were (sense): 5'-TTCCTATCTCCATCGGCATC-3' and (antisense): 5'-ATCCGTGATGACTTCCTTGG-3'. Primers for reference gene ribosomal RNA (rRNA) were (sense): 5' GACCATAAACGAT-GCCGACT 3' and (antisense); 5'-GTGAGGTTTCCCGTGTTGAG-3' (IDT, Coralville, IA).

The C_T values for rRNA were highly reproducible between samples and between PCR reactions. Although we usually considered C_T values less than 35 as specific amplification, C_T values for both KCC2 and VGAT genes in experimental and control groups were in the range of 22–26 in this study. A no template control PCR reaction was run as a negative control. cDNA preparations (n=5–6/group) were used and results were expressed as relative mRNA expression in terms of C_T values in relation to the amount of reference gene mRNA expression using formula = $2^{-(C_T\text{target} - C_T\text{rRNA})}$.

2.10 KCC2 and VGAT protein expression in spinal dorsal horn neurons (L6-S1) by Western blot analysis

Western blot analysis was carried out to investigate the long-term KCC2 and VGAT protein expression in spinal dorsal horns samples from adult rats (P60) following neonatal zymosan/saline treatments at P14–P16. The method used for Western blot analysis was as described in our previous publication [35]. In brief, approximately 10 to 25μg of spinal tissue extracts were electrophoresed by 8% SDS-PAGE and transferred onto nitrocellulose membrane. After transfer, the membrane was blocked with 5% nonfat milk and then incubated separately with rabbit anti-KCC2 (1:500; Millipore, Billerica, MA) and rabbit-anti VGAT (1:250, Alomone Labs, Jerusalem, Israel) overnight at 4°C. The membranes were then treated with secondary antibody horseradish peroxidase-conjugated goat anti-rabbit antibody (1:5000, Jackson Immuno-Research, West Grove, PA) for 2hr at room temperature. The antigen-antibody reaction was visualized using an enhanced chemiluminescent detection system (Thermo Fisher Scientific). The expression for KCC2 and VGAT was normalized against the expression of housekeeping gene β-actin for the same tissue samples using NIH ImageJ software. The relative intensity of expression against β-actin was compared between the groups (n=3/group) using the student *t* test and presented as mean± SD. Values with $p<0.05$ were considered to be significant.

2.11 *In situ* hybridization (ISH) and immunohistochemical (IHC) staining of spinal cords (L6-S1) for dual expression of miR-92b-3p and GABA-associated pre- and post-synaptic proteins

For dual ISH and IHC staining, we first carried out miR-92b-3p probe hybridization as mentioned in the ISH protocol of the method section 2.8. After completing the treatment with anti-digoxigenin-fluorescence (1:500, Roche) for 2hr at room temperature, spinal cord tissue sections were incubated overnight with either one of the following antibodies at 1:100 dilution, rabbit anti-KCC2 (Millipore), rabbit anti-VGAT (Alomone Labs) and rabbit anti-$GABA_{A\text{-}\alpha1}$ (Alomone Labs). The tissue sections were then incubated with secondary antibody goat anti-rabbit - Alexa 568 (1:500, Molecular Probes, Thermo Fisher Scientific). Slides were examined under an upright Olympus Fluoview FV1000MPE microscope (Olympus, Waltham, Massachusetts) running FV-ASW10 (version 04.02.02.09) and equipped with a 60× objective.

2.12 Surgical procedure

The implantation of EMG recording electrodes and catheter were performed in rats under deep anesthesia by injecting sodium pentobarbital (50mg/kg. i.p.). A pair of teflon-coated electrodes (Conner Wire, Part No. A5631, Chatsworth, CA, USA) were implanted into the

external oblique muscle of the abdomen and externalized through the neck for electromyography (EMG) recordings [10]. For intrathecal (i.t.) lentivirus injection at L6-S1 segment of the spinal cord, a polyethylene catheter was chronically implanted into the epidural space as reported previously [3]. All surgical procedures were carried one week (P54) before administration of i.t. lentiviral miR-92b-3p sponge or scramble miRNA into the animals.

2.13 Neuron specific lentiviral miR-92b-3p sponge for *in vivo* transfection of spinal neurons

miRNA sponge lentivirus with 6 inhibitor sequences was generated for mmu-miR-92b-3p (Accession: mmu-miR-92b-3p) and the sponge miR-92b-3p sequence was verified by PCR amplification (Creative Biogene, Shirley, NY). miR-92b-3p sponge and the control scramble miRNA sequences were then cloned under neuron specific promoter synapsin 1 in lentiviral expression vector which also expressed GFP under CMV promoter. A viral titer of 1×10^9 IFU was used for our *in vivo* study. For behavioral studies, 3 groups of adult rats at P60 were used and a schematic representation of the lentivirus treatment protocol is shown in Fig. 1B. The baseline VMR and von Frey withdrawal reflex were carried out for all animals before the induction of cystitis. As shown in Fig. 1B, rats in groups 2 and 3, received i.t. administration (L6-S1 region) of pLSyn miR-92b-3p sponge and pLSyn scramble miRNA respectively (3 μl of 1×10^9 IFU lentivirus/ml along with 1.5μl of 20ng/μl polybrene/day) for three consecutive days. Following 2 weeks interval after lentivirus treatment, all 3 groups received intravesical zymosan treatment for 3 consecutive days. The post-zymosan VMR and von Frey recordings were carried out 24hr after the last zymosan treatment to evaluate the effect of miR-92b-3p sponge on the development of visceral hyperalgesia following the induction of cystitis.

2.14 Viscero-motor (VMR) recording to colon distension

Seventy-two hours after the surgery, rats were placed inside plexiglass restraining tubes two times a day for 2hr (1 hour/session) to acclimate them to experimental conditions. The increase in EMG activity to colorectal distension (CRD) was used as an objective measure of visceral sensation and mentioned as viscero-motor response (VMR). Isobaric graded (constant pressure) distensions (10, 20, 30, 40, and 60 mmHg for 30 sec duration) were delivered with a 180 second inter-stimulus time interval. For rats in three groups, base-line VMR to graded CRD was carried out before zymosan administration. The procedure was repeated after zymosan treatment for each animal in all three groups. In each rat, the EMG activity to colon distension was measured as the area under the curve and the value was normalized to maximum response at distending pressure of 60mmHg.

2.15 Abdominal referral responses to mechanical probing

Abdominal muscle tender pain was measured in all rats of three protocols. This subjective measurement was performed using the assessment method described previously [13]. Briefly, calibrated von Frey filaments were used to test the referred somatic pain of suprapubic muscle tenderness to mechanical probing. Individual rats were placed in a lucite cubicle with a wire mesh bottom and were given 10 minutes to acclimate before testing. A series of 8 monofilaments with different forces in grams (0.02, 0.07, 0.17, 1.19, 2.05, 5.50,

11.70, 29.00) was applied to the suprapubic region of the abdomen. Each monofilament was applied 10 times as a 1–2 second stimulus with an interval of approximately 10 seconds between each stimulus. The number of withdrawal responses divided by a total of 10 trials for each monofilament was recorded as the response frequency. A Sharp retraction of the abdomen, licking/scratching, and jumping were considered as withdrawal responses.

2.16 Identification and characterization of GFP positive spinal cords (L6-S1) neurons for KCC2 and VGAT expression following lentivirus treatment

Spinal cord (L6-S1) tissues from both lentivirus sponge and scramble treated rats were collected following behavioral recordings to examine the effect of the treatment on the neuronal expression of KCC2 and VGAT. To ensure the simultaneous detection of the pre- and post-synaptic proteins and also to limit the epitope-masking after tissue fixation, we carried out a brief tissue fixation with 4% paraformaldehyde for 45 min and the tissues were processed for immunostaining within 24 hours following fixation [33]. Spinal cord tissue sections were incubated overnight with rabbit anti-GFP antibody (1:100 Cell Signaling) along with either mouse anti-KCC2 (1:100, Abcam, Cambridge, MA) or mouse anti-VGAT (1:1000, Synaptic System, GmbH, Gottingen, Germany). The tissue sections were then incubated with secondary antibody donkey anti-rabbit - Alexa 488 (1:500, Molecular Probes) and goat anti-mouse Alexa 568 (1:2000, Molecular Probes). Slides were examined by laser confocal microscope (Olympus) equipped with a 60x and 100X objectives. For image analysis, the spinal regions of laminae I to III were selected from both the sponge and scramble-treated rats. For evaluating the neuron specific alteration, we selected neurons positive for synapsin 1-induced GFP expression. We used similar settings of exposure, gain and gamma adjustment for capturing images from both sponge- and scramble-treated animals. From each section, a set of z-series was acquired from the laminae I–III from one dorsal horn with each series consisting of 10 optical sections 0.5μ apart. The individual GFP positive cells were selected and intensity of membrane KCC2 expression was measured using the Image J program. For quantifying the intensity of staining, 3 animals from each group were used and the average intensity of staining from 3 sections per group was determined. The mean intensity of staining from the sponge lentivirus-treated rats were compared with scramble virus-treated controls using the student t test and presented as mean ±SD and values with $p<0.05$ were considered to be significant.

For VGAT immunostaining for each tissue section, a single optical section (the 5th in the z-series) was viewed using the Image J program. We selected a fixed region of interest (ROI) encompassing individual GFP positive cells to count VGAT stained puncta in tissue sections from both sponge and scramble-treated rats. Three to four ROIs per section were selected for counting the number of VGAT positive puncta. Three animals from each group were used and the average intensity of staining from 3 sections per group was determined. The average number of VGAT positive puncta between the groups were compared using the student t test and presented as mean±SD and values with $p<0.05$ were considered to be significant.

2.17 Statistics

RT-PCR data was analyzed by two-way ANOVA (with Protocol and Treatment as factors), and followed by all pairwise multiple comparison tests using the Holm-Sidak method. The

von Frey and VMR data were normalized by subtracting the pre-treatment values from post-treatment values and then reanalyzed using two-way repeated measures ANOVA (with treatment and force/colorectal distension as factors). *P* value <0.05 was considered significant. Results are expressed as mean ± SEM.

3. Results

Histological assessment of bladder inflammation

As reported previously, no significant changes were observed in bladder histology in neonatal zymosan-treated rats as compared to saline controls (Figs. 1C &1D) [17]. However, adult (P60) zymosan-treated rats exhibited moderate infiltration and lymphocytes aggregation as compared to saline-treated controls. In contrast, neonatal zymosan-treated rats re-challenged with zymosan in adulthood (i.e. protocol 2 rats) exhibited the most prominent tissue histology, with significantly higher neutrophilic infiltration, vascular congestion and edema of lamina propria as compared to only adult zymosan treatment (Fig. 1D, $p<0.05$).

Expression, validation, and target gene prediction of differentially expressed miRNAs in L6-S1 spinal cord of neonatally zymosan-treated rats

In this study, we examined the effect of neonatally-induced cystitis on spinal miRNA expression using miRNA PCR array from Qiagen representing miRNAs that are reported to be involved in the transduction, modulation and maintenance of pain responses in various models of neuropathic and inflammatory pain. In PCR arrays representing 84 miRNAs involved in neuropathic and inflammatory pathways, 11 miRNAs (miR-100-5p, miR203a-3p, miR-208a-3p, miR-210-3p, miR-214-3p, miR-463-3p, miR-466d, miR-665, miR-742-3p, miR-760-5p, miR-92b-3p) demonstrated 2 to 6-fold upregulation and two (miR-223-3p, miR-133a-3p) demonstrated 2-fold down-regulation in the neonatal cystitis group compared to the saline controls (Fig. 2A). To validate PCR array results, quantitative RT-PCR was carried out for the differentially expressed miRNAs using individual spinal dorsal horn samples (L6-S1) from both neonatal zymosan-treated and saline -treated controls (fig. 2B). Among the upregulated miRNAs in PCR array, the relative expression ($2^{-\Delta C_T}$) of five miRNAs were significantly higher in neonatal cystitis rats, for miR 466d, miR-742-3p and miR-92b-3p, $*p<0.05$ and for miR-203a-3p and miR-760-5p, $**p<0.01$ vs saline-treated rats. Whereas, among the downregulated miRNAs in PCR array, the relative expression ($2^{-\Delta C_T}$) of miR-223-3p in neonatal cystitis group exhibited a trend towards down-regulation compared to saline-treated controls (p=0.06). Therefore, quantitative RT-PCR analysis of the miRNA expression profiles in individual samples validated the results obtained by PCR arrays of pooled samples in experimental and control groups.

The validated miRNAs were then subjected to targets gene prediction using three independent miRNA target prediction databases as mentioned in method section 2.6. Since our objective was to identify miRNAs with 3'UTR binding sites for genes involved in GABAergic neurotransmission, we looked for target genes associated with expression of $GABA_A$ and Glycine receptor subunits, GABA co-transporters and transporters and GABA synthesizing enzymes (Fig. 2C). In target gene analysis, these differentially expressed

miRNAs demonstrated multiple 3'UTR binding sites for several members of solute carrier gene families such as slc6, slc12, slc32, GABA receptor subunit genes and GABA synthesizing enzymes. Among the upregulated miRNAs in neonatal-cystitis rats, miR-92b-3p demonstrates multiple complementary binding sites for slc12a5, encoding K^+-coupled chloride cotransporter 2 (KCC2) and one binding site each for slc32a1 (encoding VGAT) and GABA synthesizing enzyme gad1. However, in our preliminary study, zymosan treatment protocols failed to show significant difference in gad 1 expression between experimental and control groups, suggesting that the spinal gad 1 expression is not post-transcriptionally regulated by miR-92b-3p in this rat model of zymosan-induced cystitis.

miR-92b-3p expression in L6-S1 spinal cord for all three protocols

Using RT-PCR, we further examined the expression profile of miR-92b-3p in spinal dorsal horns (L6-S1) from rats in protocol 2 and protocol 3 to evaluate whether the induction of cystitis in adulthood also has the similar effect on spinal miRNA expression (Figs. 3 A–C). As seen in neonatal cystitis rats, the relative expression ($2^{-\Delta C_T}$) of miR-92b-3p in neonatal cystitis followed by adult re-challenge and adult cystitis rats was significantly higher compared to saline-treated controls (**p<.0.01, *p<0.05 respectively vs controls).

We investigated the effect of neonatal cystitis on the expression of miR-92b-3p in lumbosacral spinal cord (L6-S1) tissue by ISH. As shown in Fig. 3D, the integrated intensity of miR-92b-3p expression in spinal dorsal horn neurons of rats with neonatal cystitis demonstrated a significant upregulation compared to saline-treated controls (**p<0.01). At the same time, there was a trend towards an increase in miR-92b-3p positive spinal dorsal horn neurons in neonatal cystitis rats with the number of miR 92b-3p expressing cells in zymosan group was 34.0± 8 compared to 22.0 ± 1.0 for saline-treated controls, p=0.06 *vs* saline controls).

KCC2 and VGAT are the potential targets for miR-92b-3p

As shown in Figure 4A, Target prediction by TargetScan identified 4 binding sites for miR-92b-3p on KCC2's 3'UTR region; 227–233 (poorly conserved 7mer-1A), 1782–1789 (conserved 8 mer), 1876–1882 (conserved 8 mer) and 2206–2212 (conserved 7mer-m8). While, MIRDB database localized 2 binding sites for miR-92b-3p (3'CACGUUA 5') on KCC2 3'UTR at seed locations 1684 & 1778 and microRNA.org identified 2 binding sites at seed location 1670 (miRSVR score-0.70) and 1764 (miRSVR score-0.91). For VGAT's 3'UTR region, MIRDB database identified one binding site at seed location 596–602 (fig. 4B) and microRNA.org and TargetScan identified a binding site at seed location 582 (miRSVR score-1.16).

To confirm that 3'UTRs of KCC2 and VGAT are the targets for miR-92b-3p, we constructed individual pEZX-MT06 reporter vectors carrying 3'UTR regions of either KCC2 or VGAT fused downstream of firefly luciferase gene and carried out in vitro transfections of HEK293T cells and dual luciferase reporter assay (Fig. 4C). HEK293 cells co-transfected with plasmid carrying KCC2 3'UTR and MIRDIAN miR-92b-3p mimic exhibited significant reduction in firefly luciferase activity compared with cells co-transfected with the same plasmid and MIRIDIAN miRNA mimic negative control (**p<0.001 vs control

plasmids). The percent reduction in firefly luciferase activity for cells co-transfected with reporter vector carrying KCC2 3'UTR and miR-92b-3p mimic was 80% in comparison with 100% activity for cells transfected with reporter vector carrying KCC2 3'UTR. The luciferase activity of cells co-transfected with vector carrying KCC2 3'UTR and miRNA mimic negative control was comparable with cells transfected only with plasmid carrying KCC2 3'UTR. For the VGAT gene, co-transfected with plasmid carrying VGAT 3'UTR and MIRDIAN miR-92b-3p mimic exhibited significant reduction in firefly luciferase activity compared with cells co-transfected with plasmid carrying VGAT 3'UTR (Fig 4C, $*p<0.01$ vs VGAT 3'UTR plasmid). However, the reduction in luciferase activity was about 50% in comparison to 80% reduction in activity for cells transfected with plasmid carrying KCC2 3'UTR. This could be due to the presence of only one complementary binding sites in the 3'UTR region of VGAT transcript, whereas, KCC2 carries 4 binding sites for miR-92b-3p in the 3'UTR region. As seen with KCC2 3'UTR plasmid, the luciferase activity of cells co-transfected with vector carrying VGAT 3'UTR and miRNA mimic negative control was comparable with cells transfected only with plasmid carrying VGAT 3'UTR (fig. 4C).

Down-regulation of KCC2 and VGAT in spinal dorsal horn (L6-S1) neurons following zymosan-induced cystitis

We next examined the effect of neonatal and adult zymosan treatments on KCC2 and VGAT gene expression in spinal dorsal horns (L6-S1) using all 3 protocols as described in Fig. 1A. The neonatal cystitis group demonstrated a long-term down-regulation of KCC2 mRNA in adult spinal cord as measured at P60 which was significantly lower than in saline-treated controls (Fig. 5A, $*p<0.05$ *vs* controls). Neonatal cystitis followed by re-challenge and adult cystitis groups also demonstrated significant down-regulation in spinal KCC2 expression compared to saline-treated controls (Figs. 5B & 5C, $*p<0.05$ *vs* controls). However, no significant difference was observed in VGAT expression in neonatal cystitis rats as compared to saline-treated controls (fig. 5A). On the other hand, re-challenge and adult cystitis groups exhibited significant down-regulation in VGAT expression (figs. 5B & C, $*p<0.05$ *vs* controls). Two-way ANOVA showed no difference in the mean expression levels of KCC2 and VGAT as obtained through quantitative RT-PCR in L6-S1 spinal cord in the three different protocols. There was no significant protocol × treatment (saline or zymosan) interaction. The long-term upregulation of spinal miR-92b-3p expression in neonatal treatment groups (protocol 1) prompted us to examine the expression of its two main target proteins, post-synaptic KCC2 and pre-synaptic VGAT in the spinal neurons from rats that only received neonatal zymosan or saline treatment (Fig. 5D). By Western blot analysis, spinal KCC2 appeared as a dimer in the molecular weight range of 122–215 KD and VGAT expression was at the range of 58–60 KD (Fig. 5D). The relative expression of KCC2 to β-actin significantly decreased in cystitis rats (0.70 ± 0.23) compared to saline-treated controls (1.29 ± 0.25, n=3/group, $*p<0.05$). The relative expression of VGAT was also significantly down-regulated in cystitis rats (0.558 ± 0.14) compared to saline-treated controls (0.913 ± 0.14, n=3/group, $*p<0.05$).

miR-92b-3p co-expression with several pre- and post-synaptic GABA-associated proteins

In dual ISH and IHC experiments, miR-92b-3p demonstrated co-expression with its target KCC2 in the spinal (L6) dorsal horn neurons (closed arrows, Fig 6D). However, KCC2

staining was predominantly on neuronal membranes with miR-92b-3p present both in membrane and cytoplasm. The post-synaptic expression of miR-92b-3p is also evident from its co-expression with $GABA_{A\text{-}\alpha1}$ positive neurons in the spinal cord (closed arrows, Fig. 6H). At the pre-synaptic level, miR-92b-3p co-expressed with several VGAT positive GABAergic boutons (closed arrows, Fig. 6L). However, the majority of VGAT staining was closely apposed to miR-92b-3p expression (open arrows, Fig. 6L).

Attenuation of the development of zymosan-induced visceral hyperalgesia following Intrathecal lentiviral sponge administration

We extended our study to investigate whether preemptive administration of miR-92b-3p sponge could attenuate the development of zymosan-induced visceral hyperalgesia in rats. The representative EMG tracings to CRD (40 and 60 mmHg) before and after zymosan treatment for naïve rats is shown in Fig. 7A. Figures 7B and 7C illustrate pre- and post-zymosan EMG tracings of rats receiving preemptive sponge miR-92b-3p and scramble miRNA, respectively. In naïve rats, post zymosan EMG responses to CRD were significantly higher compared to pre-zymosan recordings (Fig. 7D, *p<0.05, **p<0.01 *vs* pre-zymosan baseline). On the other hand, miR-92b-3p inhibitors delivered as lentivirus sponge could attenuate the development of visceral hyperalgesia when administered preemptively before inducing cystitis (Fig. 7E). In contrast, the scramble miRNA delivered through the same route failed to attenuate the EMG responses to CRD as indicated by a significantly higher VMR response to graded CRD following zymosan treatment, (Fig. 7F, * p<0.05 *vs* pre zymosan baseline). The two-way repeated measure ANOVA for lentiviral treatment demonstrated a significant difference between sponge vs naïve (p=0.002) and scramble (p=0.003).

Attenuation of zymosan-induced referred viscerosomatic hypersensitivity following intrathecal lentiviral sponge (miR-92b-3p inhibitor) administration

Intravesical zymosan administration produced an increase in viscerosomatic hypersensitivity, as indicated by a significant increase in response frequencies when von Frey filaments of increasing forces were applied to the suprapubic region of the abdomen (Fig. 8A, * p<0.05 vs pre zymosan baseline values). As shown in Fig. 8B, the preemptive administration of lentiviral sponge could attenuate the zymosan-induced increase in viscerosomatic hypersensitivity and showed comparable responses as pre-zymosan baseline values. Whereas, the preemptive administration of scramble miRNA failed to attenuate the development of viscerosomatic hypersensitivity (Fig. 8C, *p<0.05 vs pre-zymosan baseline values) induced by zymosan exposures. Our two-way repeated measure ANOVA for lentiviral treatment demonstrated a significant difference between sponge vs naïve (p<0.001) and sponge vs scramble (p<0.001).

Intrathecal preemptive lentiviral sponge administration attenuates the development of cystitis-induced spinal KCC2 and VGAT down-regulation

The spinal cord samples were collected from lentivirus-treated groups for immunostaining of KCC2 and VGAT after the completion of behavioral recordings. The preemptive administration of miR-92b-3p sponge resulted a significant upregulation of KCC2 expression in GFP-positive spinal dorsal horn neurons in L6-S1 segment compared to

preemptively scramble miRNA-treated rats (Fig 8D). Single optical section showing strong membrane - KCC2 staining for sponge-treated compared to weak staining for scramble miRNA-treated controls (arrows, Fig. 8D). Similarly, miR-92b-3p sponge administration demonstrated significant increase in VGAT positive puncta in the selected ROIs around GFP positive neurons compared to scramble miRNA-treated rats (Fig. 8E). Single optical section showing an increase in number of VGAT positive puncta around GFP-positive neurons in sponge-treated (arrows, Fig. 8E) compared to scramble-miRNA-treated rats (arrows, Fig. 8E). Quantification of the intensity of membrane KCC2 staining for GFP positive cells and the number of VGAT positive puncta around GFP positive neurons showed an increase for miR-92b-3p sponge-treated rats (Fig. 8F, for KCC2 $*p<0.01$, VGAT $**p<0.001$ vs scramble miRNA).

4. Discussion

In the present study, we report for the first time that in experimental models of zymosan-induced cystitis, the increased spinal miR-92b-3p expression contributes to chronic pelvic pain and visceral nociception by downregulating two of its target genes: GABA-associated transporters KCC2 and VGAT in LS spinal dorsal horn neurons. Both neonatal and adult bladder inflammation protocols demonstrated similar increase in spinal miR-92b-3p expression and subsequent decrease in KCC2 and VGAT gene expression indicating a major role for miR-92b-3p-mediated transcriptional dysregulation of spinal GABAergic transmission in pathophysiology of zymosan-induced cystitis and bladder pain syndrome. Using *in situ* hybridization, we demonstrated a significant upregulation of miR-92b-3p in the spinal dorsal horn neurons of neonatal cystitis rats compared with saline-treated controls. In a subsequent dual *in situ* hybridization and immunohistochemistry study, we further confirmed the co-expression of miR-92b-3p with targets for KCC2 and VGAT in spinal dorsal horn neurons, emphasizing a possible regulatory role of this miRNA on spinal GABAergic transmission both at pre- and postsynaptic levels. We then demonstrated that inhibiting miR-92b-3p expression in L6-S1 spinal neurons by intrathecal administration of lentiviral pLSyn-miR-92b-3p sponge (carrying miR-92b-3p inhibitor) upregulates spinal KCC2 and VGAT expression in spinal dorsal horn neurons. In behavioral studies, intrathecal administration of lentiviral miR-92b-3p sponge in lumbosacral region in rats before inducing cystitis reduced visceral hyperalgesia and referred viscerosomatic hypersensitivity compared to group receiving scramble lentivirus. Considering that we used neuronal synapsin promoter for selective expression miR-92b-3p sponge, our findings demonstrate the specific relevance of miR-92b-3p-mediated down-regulation of GABAergic transmission in the spinal neurons as a major contributor towards the pathophysiology of zymosan-induced CPP.

miRNAs have recently emerged as major transcriptional regulators of gene expression and appear to regulate the expression of various receptors and neurotransmitters in the CNS. Several studies support the involvement of miRNA-mediated gene regulation in pathophysiology of acute and chronic pain [1; 4; 8; 12; 18; 23; 30; 31; 40; 42]. At the synaptic level, miRNAs specifically target neuronal mRNAs localized near the synapse and modulate input-specific synaptic protein synthesis and neuronal plasticity [22; 28]. We previously reported the involvement of spinal miR-181a in both transcriptional as well as translational repression of spinal $GABA_{A\alpha\text{-}1}$ receptor subunit expression in adult rats

following neonatal bladder inflammation [35]. The miRNA PCR array findings in our present study further validate the presence of common miRNA-mediated gene regulatory mechanisms between zymosan-induced bladder pain and/or cystitis and other neuropathic and inflammatory pain processes. Although previous studies have shown the involvement of miR-92 in post-transcriptional regulation of GABAergic transmission in cerebellar granule neurons and hippocampal memory formation in mice, to our knowledge this is the first report indicating spinal miR-92b-3p in transcriptional dysregulation of GABAergic transmission and development of visceral hyperalgesia in zymosan-induced cystitis [2; 38]. In a recent study, miR-92a-mediated down-regulation of VGAT expression in the hippocampus CA3 region has been implicated as the molecular mechanism of underlying anxiety in patients with Alzheimer's disease [15]. Although both miR-92a and miR-92b-3p carry identical complementary binding sites for VGAT 3'UTR transcript, however, miR-92a expression was comparable between zymosan and saline-treated rats in the present study. This could be due to the presence of brain-region specific miRNA biogenesis and the involvement of distinct miRNA-mediated post-transcriptional gene regulatory mechanism for different disease processes.

In the spinal cord, primary afferent neurons from the periphery makes synaptic connection with the projection neurons and interneurons located in superficial lamina I and II and around 25–40% of spinal neurons are reported to be GABAergic in laminae I–III [19; 24; 37]. The loss of GABAergic inhibition in pain-signaling pathways has been proposed as one of the primary mechanisms for pain-induced hyperalgesia and appear to play a key role in the development of acute to chronic pain [11; 19]. Impaired GABAergic inhibition in the spinal cord has been reported to contribute to neuropathic pain characterized by increased sensitivity to thermal and mechanical stimuli [25; 32]. The mechanism of underlying impaired GABAergic inhibition in pain pathophysiology is not fully understood but a number of different mechanisms have been proposed which may include impairment in expression and function of various GABA-associated components both at presynaptic and postsynaptic levels, such as $GABA_A$ receptor subunits, co-transporter KCC2, GABA synthesizing enzymes (Gad1 and Gad2), and GABA transporters [10; 19; 34]. Our present findings along with our previous report suggest that the spinal GABAergic impairment in the setting of zymosan-induced bladder pain syndrome is mediated through miRNA-mediated epigenetic regulation of various GABA-associated receptors, transporters and co-transporters both at pre-synaptic and post-synaptic levels.

The involvement of KCC2-mediated impairment of spinal (Cl^-) homeostasis has been reported in rats with chronic water avoidance stress (WAS)-induced visceral hyperalgesia [36]. Similarly, in a nerve injury model, intrathecal delivery of KCC2 using lentiviral vector results in a complete and long-lasting reversal of pain hypersensitivity by restoring Cl^- homeostasis both at spinal and peripheral levels [14]. Unlike KCC2, the role of VGAT in pathophysiology of GABA disinhibition is not clearly defined. However, in heterozygous VGAT(+/−) mice, the thermal nociception and inflammatory pain sensation are greater compared to wild-type (WT) mice, indicating the role of VGAT-mediated inhibitory drive in specific forms of sensory pain processing [39]. In addition, electrophysiological recording of spinal motor neurons from VGAT knockout mice during embryonic day E18.5 also exhibits no spontaneous inhibitory postsynaptic current mediated by GABA [29]. In line with these

observations, our present study also suggests that the spinal sensitization in zymosan-induced cystitis could be due to reduced expression of two important components of GABAergic transmission namely KCC2 and VGAT in the spinal dorsal horn neurons.

Several preclinical studies have demonstrated that the exposure to bladder inflammation early-in-life can cause long-term alteration in sensory pain processing during adulthood [6; 17; 26]. We have recently demonstrated a long-term down-regulation of $GABA_{A\alpha\text{-}1}$ receptor subunit expression in spinal neurons following neonatal cystitis and intrathecal administration of $GABA_A$ receptor agonist muscimol that failed to attenuate the visceromotor response in these hyperalgesic rats indicating an impairment of postsynaptic GABA transmission [35]. Similarly, we have also shown that the intrathecal administration of HZ166, a potent $GABA_{A\alpha\text{-}2}$ agonist, is ineffective in attenuating both VMR and UBD responsive spinal neurons in rats with neonatal cystitis [10]. In the present study, we further demonstrated that the intrathecal administration of miR-92b-3p inhibitor can restore the expression of KCC2 and VGAT in spinal neurons and also attenuates the development of visceral hyperalgesia in neonatal zymosan-treated rats. The adult zymosan treatment demonstrated a transient down-regulation of both KCC2 and VGAT gene expression and concomitant increase in spinal miR-92b-3p, the day after the induction of cystitis. However, unlike with neonatally-treated rats, the adult zymosan treatment failed to demonstrate a prolonged increase in pain sensitivity and down-regulation of spinal KCC2 and VGAT expression when tested 6 weeks after zymosan treatment (data not shown).

Accumulating evidence suggests the involvement of miRNAs in the underlying pathophysiology of visceral pain disorders [41; 42]. For example, colonic biopsies from patients with irritable bowel syndrome (IBS) reveal reduced miR199a/b expression in patients with diarrhea predominant IBS compared with that of normal individuals [42]. Moreover, decreased miR-199 directly correlates with increased colonic TRPV1 expression and inversely with visceral pain scores. The increase in colonic miR-29a expression has been associated with intestinal permeability in IBS patients with chronic abdominal pain [41]. In patients with bladder pain syndromes, overexpression of bladder miR-199a-5p has been linked to impaired urothelial permeability [18], and, bladder miRNAs have also been implicated in the modulation of NK1 receptor expression and the underlying molecular mechanisms of bladder pain syndrome [31]. Although we have not examined the expression pattern of miRNAs in the bladder or colon tissues of cystitis rats, histopathological evaluation of bladder tissues revealed a higher inflammatory cell infiltration, erosion, and edema in rats with neonatal zymosan and adult zymosan re-challenge compared to only adult zymosan exposures, whereas, in neonatal zymosan-treated rats without re-challenge bladder histology appeared normal. This finding indicates that underlying morphological changes occur following neonatal exposure which initiates an enhanced inflammatory response when the bladder is re-exposed to zymosan in adulthood. These heightened bladder histological changes following re-challenge are worth addressing to delineate the mechanism of early-life dependent vulnerability of long-term alteration in visceral sensory system and its contribution towards the development of bladder pain syndrome.

Overall, our study documents spinal GABAergic deregulation as one of the pathophysiologic mechanisms underlying chronic pelvic pain, which may have potential for future

development of miRNA-based therapy for IC/BPS. The present results along with our previous findings emphasize that miRNA-mediated down-regulation of spinal KCC2, VGAT and $GABA_A$ receptor subtypes in cystitis rats may be a potential factor for increased visceral hypersensitivity and the development of chronic pelvic pain. In *in vivo* studies, we have also shown that miR-92b-3p inhibitor could be used successfully to dampen visceral hypersensitivity and upregulate KCC2 and VGAT expression in the spinal cord. In the future, miRNA-based strategies may be useful to reverse the GABAergic inhibitory modulation which appears to be one of the major underlying mechanisms leading to CPP.

Acknowledgments

This work was supported by NIH R01DK099201-01A1 grant awarded to Drs. B. Banerjee and J. N. Sengupta. We greatly appreciate Marie Schulte, Ph.D., imaging specialist, at the Blood Research Institute's (Southern Wisconsin) Northwestern Mutual Microscopy Core facility for her assistance with the confocal imaging.

References

1. Aldrich BT, Frakes EP, Kasuya J, Hammond DL, Kitamoto T. Changes in expression of sensory organ-specific microRNAs in rat dorsal root ganglia in association with mechanical hypersensitivity induced by spinal nerve ligation. Neuroscience. 2009; 164(2):711–723. [PubMed: 19699278]
2. Barbato C, Ruberti F, Pieri M, Vilardo E, Costanzo M, Ciotti MT, Zona C, Cogoni C. MicroRNA-92 modulates K(+) Cl(−) co-transporter KCC2 expression in cerebellar granule neurons. J Neurochem. 2010; 113(3):591–600. [PubMed: 20050974]
3. Chen L, Jiang M, Pei L. Comparison of three methods of drug delivery in the rat lumbar spinal subarachnoid space. Anat Rec (Hoboken). 2012; 295(7):1212–1220. [PubMed: 22674909]
4. Ciszek BP, Khan AA, Dang H, Slade GD, Smith S, Bair E, Maixner W, Zolnoun D, Nackley AG. MicroRNA expression profiles differentiate chronic pain condition subtypes. Transl Res. 2015; 166(6):706–720. e711. [PubMed: 26166255]
5. Coull JA, Boudreau D, Bachand K, Prescott SA, Nault F, Sik A, De Koninck P, De Koninck Y. Trans-synaptic shift in anion gradient in spinal lamina I neurons as a mechanism of neuropathic pain. Nature. 2003; 424(6951):938–942. [PubMed: 12931188]
6. DeBerry J, Ness TJ, Robbins MT, Randich A. Inflammation-induced enhancement of the visceromotor reflex to urinary bladder distention: modulation by endogenous opioids and the effects of early-in-life experience with bladder inflammation. J Pain. 2007; 8(12):914–923. [PubMed: 17704007]
7. Hasbargen T, Ahmed MM, Miranpuri G, Li L, Kahle KT, Resnick D, Sun D. Role of NKCC1 and KCC2 in the development of chronic neuropathic pain following spinal cord injury. Ann N Y Acad Sci. 2010; 1198:168–172. [PubMed: 20536931]
8. He Y, Yang C, Kirkmire CM, Wang ZJ. Regulation of opioid tolerance by let-7 family microRNA targeting the mu opioid receptor. J Neurosci. 2010; 30(30):10251–10258. [PubMed: 20668208]
9. Jolivalt CG, Lee CA, Ramos KM, Calcutt NA. Allodynia and hyperalgesia in diabetic rats are mediated by GABA and depletion of spinal potassium-chloride co-transporters. Pain. 2008; 140(1): 48–57. [PubMed: 18755547]
10. Kannampalli P, Babygirija R, Zhang J, Poe MM, Li G, Cook JM, Shaker R, Banerjee B, Sengupta JN. Neonatal bladder inflammation induces long-term visceral pain and altered responses of spinal neurons in adult rats. Neuroscience. 2017; 346:349–364. [PubMed: 28126369]
11. Knabl J, Witschi R, Hosl K, Reinold H, Zeilhofer UB, Ahmadi S, Brockhaus J, Sergejeva M, Hess A, Brune K, Fritschy JM, Rudolph U, Mohler H, Zeilhofer HU. Reversal of pathological pain through specific spinal GABAA receptor subtypes. Nature. 2008; 451(7176):330–334. [PubMed: 18202657]
12. Kusuda R, Cadetti F, Ravanelli MI, Sousa TA, Zanon S, De Lucca FL, Lucas G. Differential expression of microRNAs in mouse pain models. Mol Pain. 2011; 7:17. [PubMed: 21385380]

13. Lee UJ, Ackerman AL, Wu A, Zhang R, Leung J, Bradesi S, Mayer EA, Rodriguez LV. Chronic psychological stress in high-anxiety rats induces sustained bladder hyperalgesia. Physiol Behav. 2015; 139:541–548. [PubMed: 25449389]
14. Li L, Chen SR, Chen H, Wen L, Hittelman WN, Xie JD, Pan HL. Chloride Homeostasis Critically Regulates Synaptic NMDA Receptor Activity in Neuropathic Pain. Cell Rep. 2016; 15(7):1376–1383. [PubMed: 27160909]
15. Li X, Wang Z, Tan L, Wang Y, Lu C, Chen R, Zhang S, Gao Y, Liu Y, Yin Y, Liu X, Liu E, Yang Y, Hu Y, Xu Z, Xu F, Wang J, Liu GP, Wang JZ. Correcting miR92a-vGAT-Mediated GABAergic Dysfunctions Rescues Human Tau-Induced Anxiety in Mice. Mol Ther. 2017; 25(1):140–152. [PubMed: 28129110]
16. Mestdagh P, Lefever S, Pattyn F, Ridzon D, Fredlund E, Fieuw A, Ongenaert M, Vermeulen J, De Paepe A, Wong L, Speleman F, Chen C, Vandesompele J. The microRNA body map: dissecting microRNA function through integrative genomics. Nucleic Acids Res. 2011; 39(20):e136. [PubMed: 21835775]
17. Miranda A, Mickle A, Schmidt J, Zhang Z, Shaker R, Banerjee B, Sengupta JN. Neonatal cystitis-induced colonic hypersensitivity in adult rats: a model of viscero-visceral convergence. Neurogastroenterol Motil. 23(7):683–e281.
18. Monastyrskaya K, Sanchez-Freire V, Hashemi Gheinani A, Klumpp DJ, Babiychuk EB, Draeger A, Burkhard FC. miR-199a-5p regulates urothelial permeability and may play a role in bladder pain syndrome. Am J Pathol. 2013; 182(2):431–448. [PubMed: 23201090]
19. Moore KA, Kohno T, Karchewski LA, Scholz J, Baba H, Woolf CJ. Partial peripheral nerve injury promotes a selective loss of GABAergic inhibition in the superficial dorsal horn of the spinal cord. J Neurosci. 2002; 22(15):6724–6731. [PubMed: 12151551]
20. Morgado C, Pereira-Terra P, Cruz CD, Tavares I. Minocycline completely reverses mechanical hyperalgesia in diabetic rats through microglia-induced changes in the expression of the potassium chloride co-transporter 2 (KCC2) at the spinal cord. Diabetes Obes Metab. 2011; 13(2):150–159. [PubMed: 21199267]
21. Morgado C, Pinto-Ribeiro F, Tavares I. Diabetes affects the expression of GABA and potassium chloride cotransporter in the spinal cord: a study in streptozotocin diabetic rats. Neurosci Lett. 2008; 438(1):102–106. [PubMed: 18457921]
22. Pichardo-Casas I, Goff LA, Swerdel MR, Athie A, Davila J, Ramos-Brossier M, Lapid-Volosin M, Friedman WJ, Hart RP, Vaca L. Expression profiling of synaptic microRNAs from the adult rat brain identifies regional differences and seizure-induced dynamic modulation. Brain Res. 2012; 1436:20–33. [PubMed: 22197703]
23. Poh KW, Yeo JF, Ong WY. MicroRNA changes in the mouse prefrontal cortex after inflammatory pain. Eur J Pain. 2011; 15(8):801, e801–812. [PubMed: 21397537]
24. Polgar E, Hughes DI, Riddell JS, Maxwell DJ, Puskar Z, Todd AJ. Selective loss of spinal GABAergic or glycinergic neurons is not necessary for development of thermal hyperalgesia in the chronic constriction injury model of neuropathic pain. Pain. 2003; 104(1–2):229–239. [PubMed: 12855333]
25. Price TJ, Cervero F, de Koninck Y. Role of cation-chloride-cotransporters (CCC) in pain and hyperalgesia. Curr Top Med Chem. 2005; 5(6):547–555. [PubMed: 16022677]
26. Randich A, Mebane H, DeBerry JJ, Ness TJ. Rostral ventral medulla modulation of the visceromotor reflex evoked by urinary bladder distension in female rats. J Pain. 2008; 9(10):920–926. [PubMed: 18619908]
27. Rivera C, Voipio J, Payne JA, Ruusuvuori E, Lahtinen H, Lamsa K, Pirvola U, Saarma M, Kaila K. The K+/Cl− co-transporter KCC2 renders GABA hyperpolarizing during neuronal maturation. Nature. 1999; 397(6716):251–255. [PubMed: 9930699]
28. Saba R, Storchel PH, Aksoy-Aksel A, Kepura F, Lippi G, Plant TD, Schratt GM. Dopamine-regulated microRNA MiR-181a controls GluA2 surface expression in hippocampal neurons. Mol Cell Biol. 2012; 32(3):619–632. [PubMed: 22144581]
29. Saito K, Kakizaki T, Hayashi R, Nishimaru H, Furukawa T, Nakazato Y, Takamori S, Ebihara S, Uematsu M, Mishina M, Miyazaki J, Yokoyama M, Konishi S, Inoue K, Fukuda A, Fukumoto M, Nakamura K, Obata K, Yanagawa Y. The physiological roles of vesicular GABA transporter

during embryonic development: a study using knockout mice. Mol Brain. 2010; 3:40. [PubMed: 21190592]

30. Sanchez-Simon FM, Zhang XX, Loh HH, Law PY, Rodriguez RE. Morphine regulates dopaminergic neuron differentiation via miR-133b. Mol Pharmacol. 2010; 78(5):935–942. [PubMed: 20716624]
31. Sanchez Freire V, Burkhard FC, Kessler TM, Kuhn A, Draeger A, Monastyrskaya K. MicroRNAs may mediate the down-regulation of neurokinin-1 receptor in chronic bladder pain syndrome. Am J Pathol. 2010; 176(1):288–303. [PubMed: 20008142]
32. Sandkuhler J. Models and mechanisms of hyperalgesia and allodynia. Physiol Rev. 2009; 89(2): 707–758. [PubMed: 19342617]
33. Schneider Gasser EM, Straub CJ, Panzanelli P, Weinmann O, Sassoe-Pognetto M, Fritschy JM. Immunofluorescence in brain sections: simultaneous detection of presynaptic and postsynaptic proteins in identified neurons. Nat Protoc. 2006; 1(4):1887–1897. [PubMed: 17487173]
34. Schoffnegger D, Heinke B, Sommer C, Sandkuhler J. Physiological properties of spinal lamina II GABAergic neurons in mice following peripheral nerve injury. J Physiol. 2006; 577(Pt 3):869–878. [PubMed: 17053034]
35. Sengupta JN, Pochiraju S, Kannampalli P, Bruckert M, Addya S, Yadav P, Miranda A, Shaker R, Banerjee B. MicroRNA-mediated GABA Aalpha-1 receptor subunit down-regulation in adult spinal cord following neonatal cystitis-induced chronic visceral pain in rats. Pain. 154(1):59–70.
36. Tang D, Qian AH, Song DD, Ben QW, Yao WY, Sun J, Li WG, Xu TL, Yuan YZ. Role of the potassium chloride cotransporter isoform 2-mediated spinal chloride homeostasis in a rat model of visceral hypersensitivity. Am J Physiol Gastrointest Liver Physiol. 2015; 308(9):G767–778. [PubMed: 25792562]
37. Todd AJ, Hughes DI, Polgar E, Nagy GG, Mackie M, Ottersen OP, Maxwell DJ. The expression of vesicular glutamate transporters VGLUT1 and VGLUT2 in neurochemically defined axonal populations in the rat spinal cord with emphasis on the dorsal horn. Eur J Neurosci. 2003; 17(1): 13–27. [PubMed: 12534965]
38. Vetere G, Barbato C, Pezzola S, Frisone P, Aceti M, Ciotti M, Cogoni C, Ammassari-Teule M, Ruberti F. Selective inhibition of miR-92 in hippocampal neurons alters contextual fear memory. Hippocampus. 2014; 24(12):1458–1465. [PubMed: 24990518]
39. Yamada MH, Nishikawa K, Kubo K, Yanagawa Y, Saito S. Impaired glycinergic synaptic transmission and enhanced inflammatory pain in mice with reduced expression of vesicular GABA transporter (VGAT). Mol Pharmacol. 2012; 81(4):610–619. [PubMed: 22275517]
40. Zhao J, Lee MC, Momin A, Cendan CM, Shepherd ST, Baker MD, Asante C, Bee L, Bethry A, Perkins JR, Nassar MA, Abrahamsen B, Dickenson A, Cobb BS, Merkenschlager M, Wood JN. Small RNAs control sodium channel expression, nociceptor excitability, and pain thresholds. J Neurosci. 2010; 30(32):10860–10871. [PubMed: 20702715]
41. Zhou Q, Souba WW, Croce CM, Verne GN. MicroRNA-29a regulates intestinal membrane permeability in patients with irritable bowel syndrome. Gut. 2010; 59(6):775–784. [PubMed: 19951903]
42. Zhou Q, Yang L, Larson S, Basra S, Merwat S, Tan A, Croce C, Verne GN. Decreased miR-199 augments visceral pain in patients with IBS through translational upregulation of TRPV1. Gut. 2016; 65(5):797–805. [PubMed: 25681400]

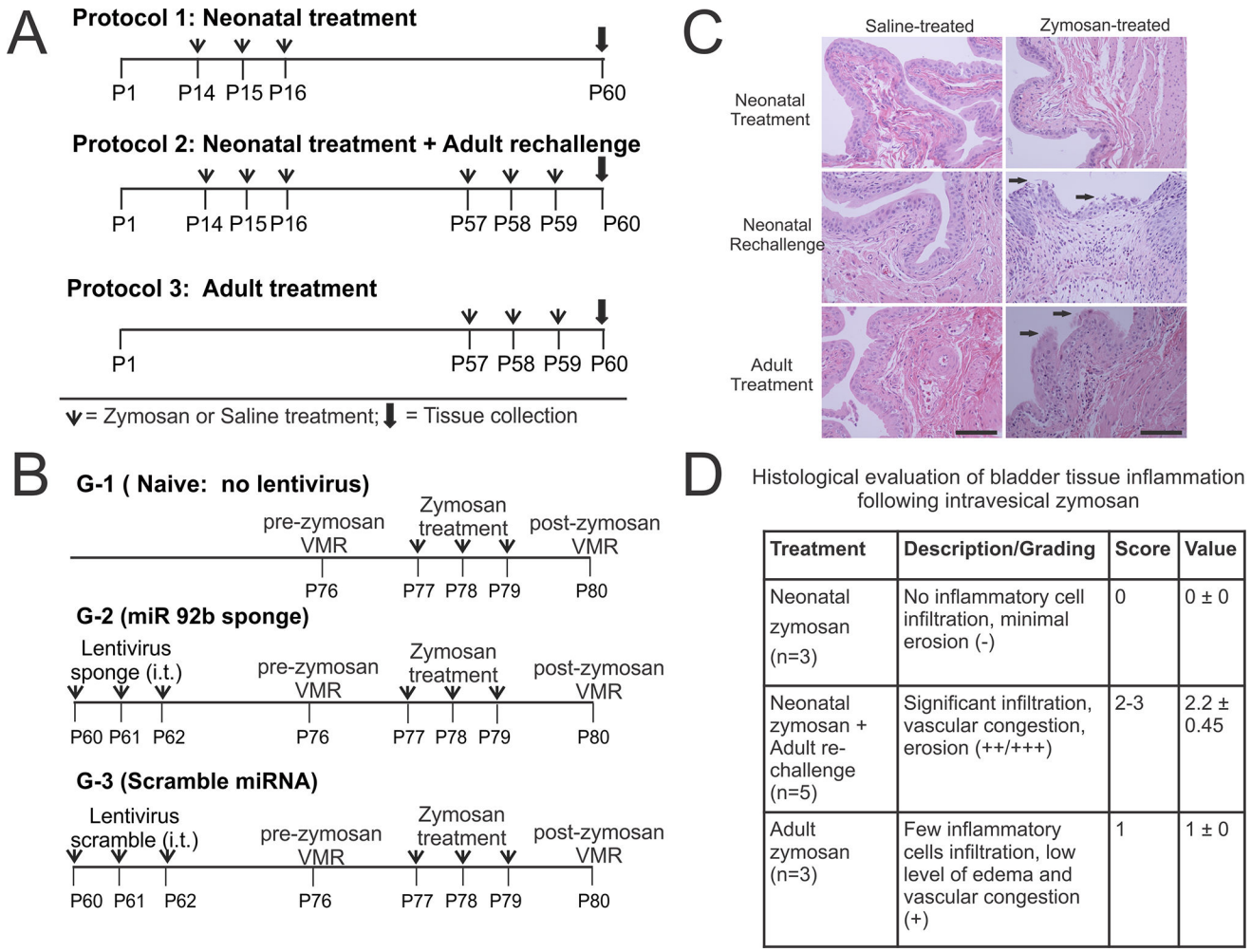

D

Histological evaluation of bladder tissue inflammation following intravesical zymosan

Treatment	Description/Grading	Score	Value
Neonatal zymosan (n=3)	No inflammatory cell infiltration, minimal erosion (-)	0	0 ± 0
Neonatal zymosan + Adult re-challenge (n=5)	Significant infiltration, vascular congestion, erosion (++/+++)	2-3	2.2 ± 0.45
Adult zymosan (n=3)	Few inflammatory cells infiltration, low level of edema and vascular congestion (+)	1	1 ± 0

Figure 1.

Schematic representation of three zymosan treatment protocols used in this study. (A) In protocol 1, neonatal zymosan. In protocol 2, similar neonatal treatment as in protocol 1 followed by re-challenge with zymosan or saline at adult stage and in protocol 3, adult zymosan or saline treatment from P57 thro and tissue collection on P60. (B) Schematic representation of intrathecal Lentiviral sponge and scramble miRNA administration preemptively before inducing cystitis in adult rats. (C) Histological examination of the bladder tissues at P60 for rats in all 3 protocols. Hematoxylin and eosin staining reveals no epithelial damage and inflammation in neonatally zymosan-treated rats in protocol 1. Zymosan-treated rats in protocol 2 demonstrate the most prominent epithelial damage and inflammatory cell infiltration among the three treatment protocols. Arrows indicate urothelial damage. Scale bar indicates 100μm. (D). Histopathological changes of the bladder tissue in protocol 2 is significantly higher than in bladder tissues from rats in protocol 3 (fig. 1D, $p<0.05$).

A miRNA PCR Array: Neonatal Cystitis vs saline controls

miRNAs	fold change
miR-100-5p	2.6
miR-133a-3p	0.5
miR-203a-3p	2.1
miR-208a-3p	4.5
miR-210-3p	2.0
miR-214-3p	2.5
miR-223-3p	0.5
miR-463-3p	5.0
miR-665	2.0
miR-466d	6.8
miR-742-3p	3.8
miR-760-5p	6.3
miR-92b-3p	2.4

B

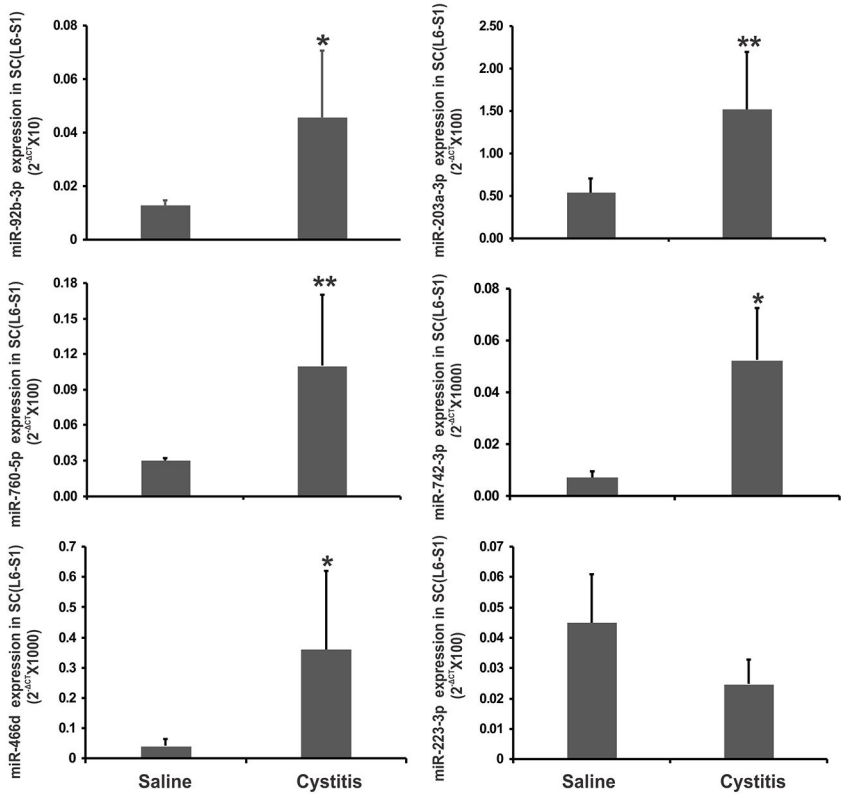

C miRNA target gene bioinformatics prediction

miR 92-3p	miR 203a-3p	miR 742-3P	miR 466d	miR 214-3p
Slc12a5, Slc32a1, Gad1, Glra1	Slc32a1, Slc12a2, Gabra1, Gabbr1, Gabbr2, Gabrr1	Slc6a1, Slc6a12, Gabra1, Gabrg1, Gabrd, Gabrr1, Gabrr3, Gria2	Gabra1, Gabrb3, Gabrr3, GABBR1, Gabrr2, Gria2, Gria3, Gria4	Slc12a3, Slc6a12
miR 208-3p	**miR 463-3p**	**miR 760-5p**	**miR 665**	**miR 100-5p**
Gabra1	Slc6a1, Slc6a5, Slc6a12, Gad1, Gria4, Grid2	Gria3, Grina, Grm1	Slc6a1, Slc6a7, Gabrr3, Grm2	Slc18a1, Glra2, Gria4

Figure 2.

miRNA expression profile and bioinformatics prediction of miRNA targets. (A) Qiagen PCR miRNA array (Neuropathic and inflammatory pain pathways) analysis of lumbosacral (L6-S1) spinal dorsal horn samples following neonatal zymosan-induced cystitis in rats. (B) Real-time RT-PCR validation of PCR array results for the differentially expressed miRNAs. The ordinate value $2^{-\Delta CT}$ corresponds to the miRNA expression relative to endogenous SNORD-95 expression and is represented as mean ± SD, n=5/group, * $p<0.05$, ** $p<0.01$ *vs* saline controls. (C) Target prediction of several GABA-associated genes with 3'UTR binding sites for miRNAs that show upregulation in cystitis rats (≥2 fold) compared to saline-treated controls.

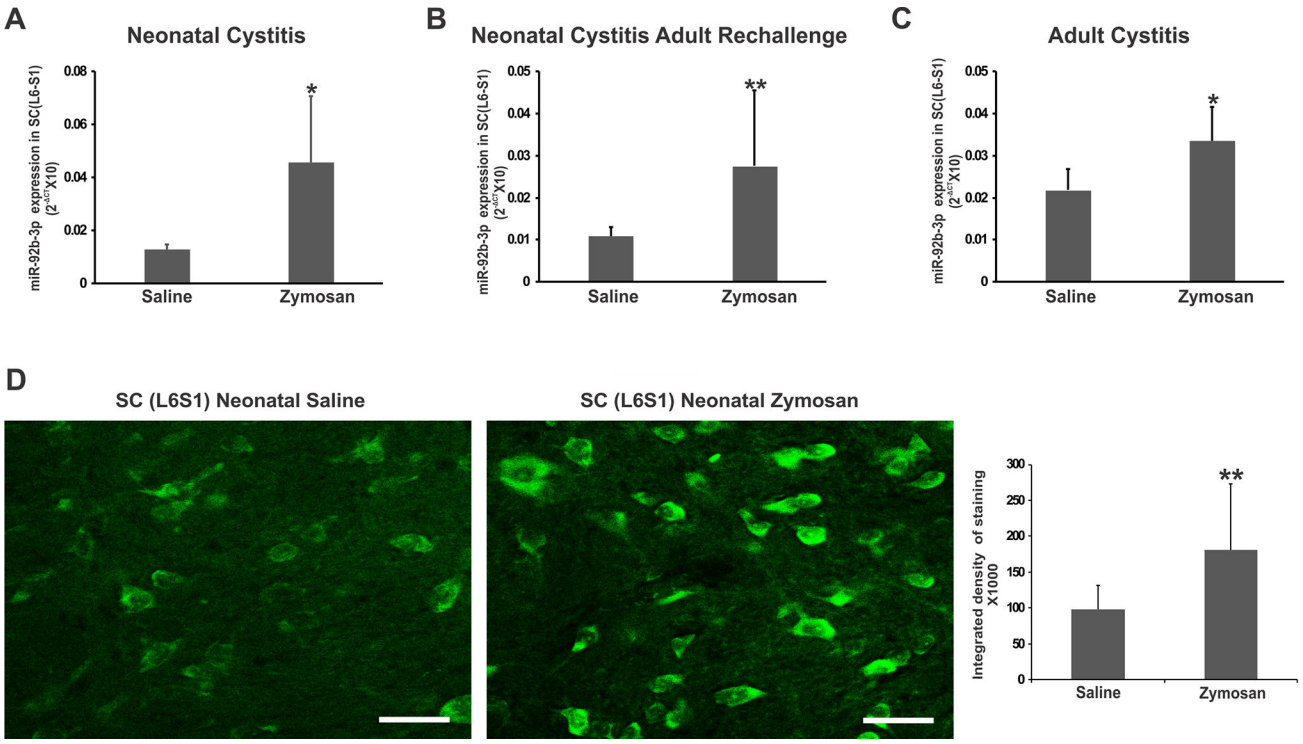

Figure 3.

miR-92b-3p expression in spinal dorsal horn (L6-S1) samples from rats receiving treatment as described in Fig. 1. Groups include: (A) neonatally-induced cystitis; (B) neonatal cystitis followed by adult re-challenge; (C) adult cystitis. The ordinate value $2^{-\Delta CT}$ corresponds to the miRNA expression relative to endogenous SNORD-95 expression and is represented as mean ± SD, n=5/group, * $p<0.05$, ** $p<0.01$ vs saline controls. (D) In situ hybridization demonstrates significant upregulation of intensity of miR-92b-3p expression (** $p<0.01$ *vs* saline controls) in zymosan treated rats. The scale bar is 50 μm.

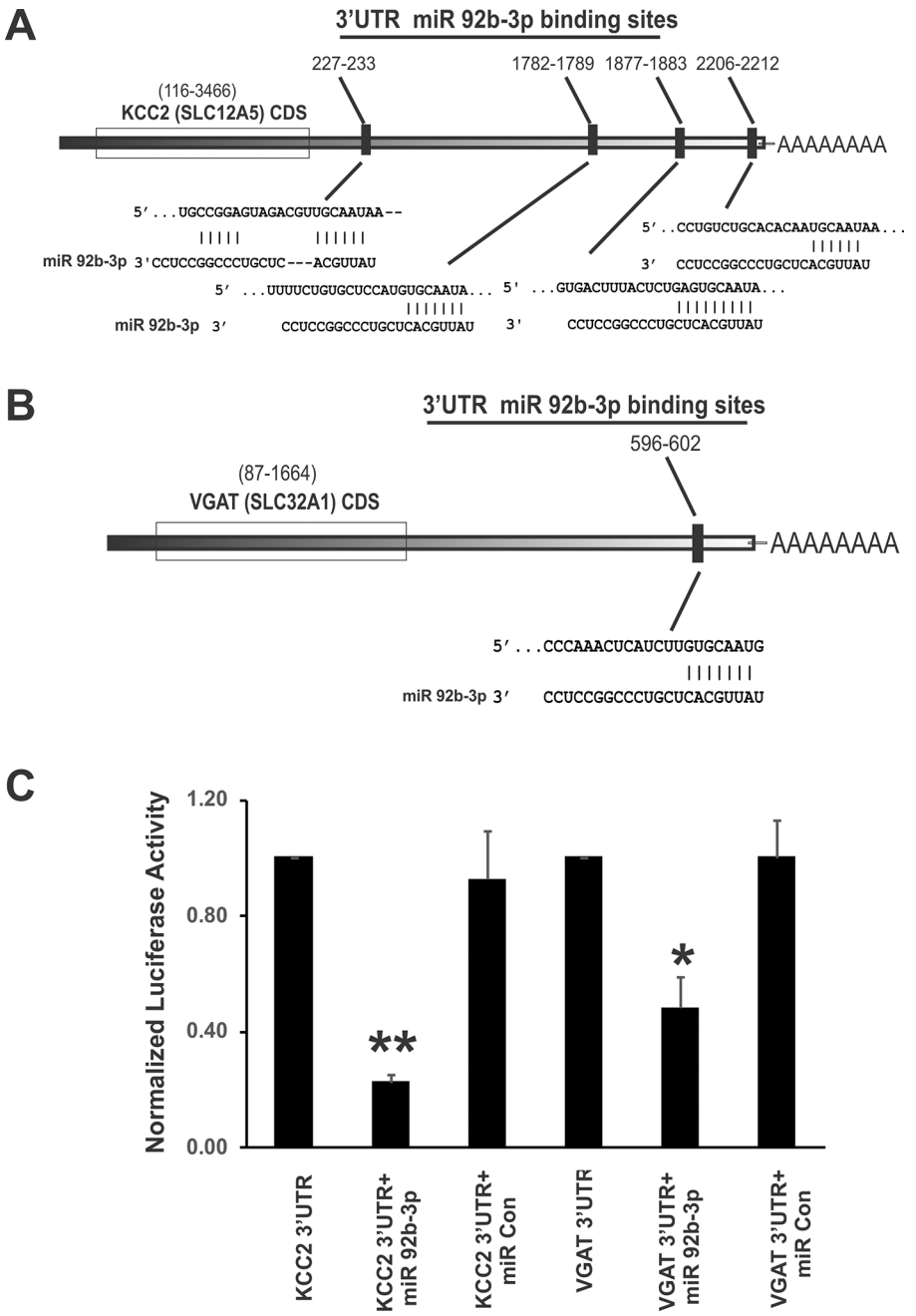

Figure 4.

Schematic representation of 3' UTR of KCC2 and VGAT mRNA with complementary binding sequences for miR-92b-3p and Luciferase Assay validation. (A) 3'UTR of KCC2 (Slc12a5 gene) mRNA demonstrates four complimentary binding sequences (response elements) for the seed region of miR-92b-3p. (B) 3'UTR of VGAT (Slc32a1 gene) mRNA carries one complimentary binding site for miR-92b-3p. (C) miR-92b-3p interaction with 3'UTRs of KCC2 and VGAT in HEK293 cells. The percentage reduction in luciferase activity of the cells transfected with plasmid carrying either KCC2 or VGAT 3'UTRs and miR-92b-3p was calculated by considering 100% luciferase activity for cells transfected

only with plasmid carrying the 3'UTR of the target gene. The data represent the normalized luciferase activity of three different sets of transfections. The percentage reduction in luciferase reduction activity of cells transfected with KCC2 3'UTR and miR 92b-3p mimic is significantly higher than cells transfected with KCC2 and miR-control mimic (fig. 4C, $^{**}p<0.001$). Similarly, percentage reduction in luciferase activity of cells transfected with VGAT 3'UTR and miR 92b-3p is significantly higher than cells transfected with VGAT and miR control mimic (fig. 4C, $^{*}p<0.01$).

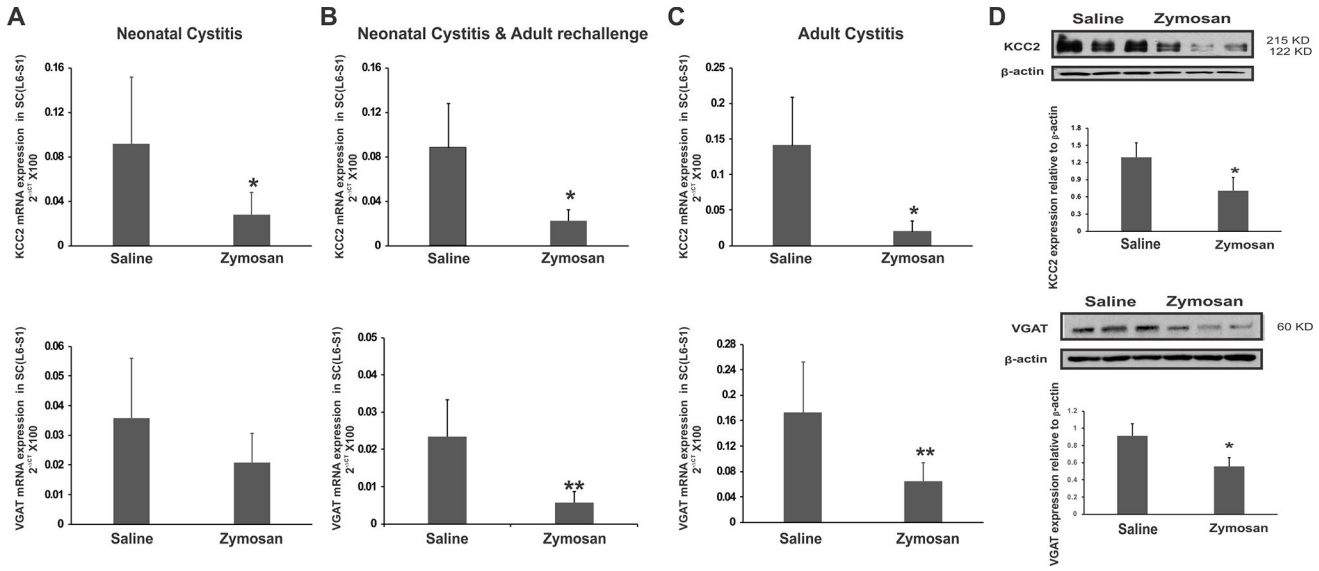

Figure 5.

The expression profile of KCC2 and VGAT mRNA and protein in spinal dorsal horns (L6-S1) from rats treated by 3 different protocols as mentioned in Fig. 1. Groups include: (A) neonatally-induced cystitis; (B) neonatal cystitis followed by adult re-challenge; (C) adult cystitis. The ordinate value $2^{-\Delta CT}$ corresponds to the mRNA expression relative to endogenous ribosomal RNA (rRNA) expression and is represented as mean ± SD, n=5/group, * $p<0.05$, ** $p<0.01$ *vs* saline controls. (D) Western Blot analysis of KCC2 and VGAT expression in spinal dorsal horn samples (L6-S1) from neonatal zymosan and saline-treated rats in protocol 1. The intensity of KCC2 and VGAT immunoreactivity is normalized against the intensity of β-actin. Results are expressed as means ± SD n=3/group, * p<0.05 vs saline controls.

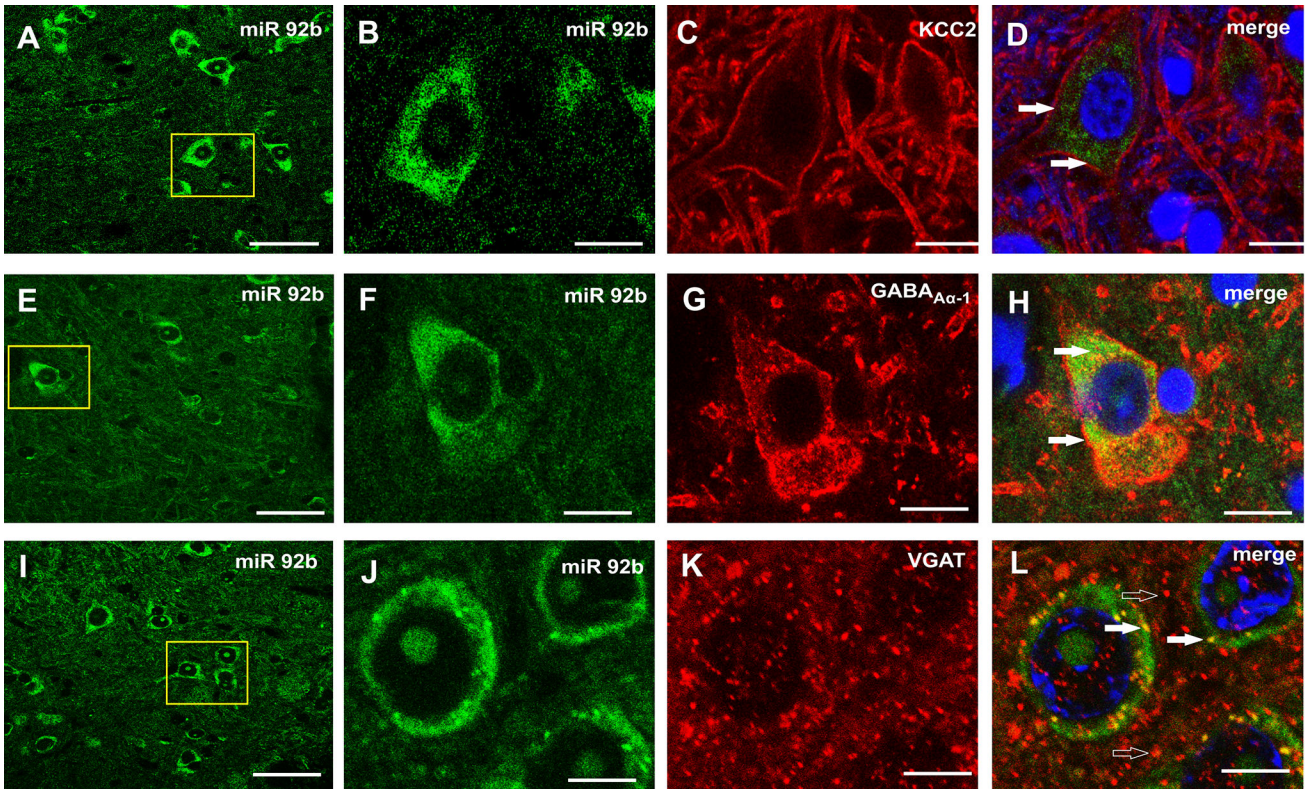

Figure 6.

Dual in situ hybridization and immunohistochemistry in spinal cord (L6-S1) demonstrate co-expression of miR-92b-3p with both presynaptic and postsynaptic GABA-associated transporters, cotransporter, receptor in spinal dorsal horn neurons. The close arrows demonstrate co-expression of miR-92b-3p (green) with KCC2 in fig. 6D and with $GABA_{A\alpha\text{-}1}$ in fig. 6H (red). The VGAT staining that are not colocalized but closely apposed to miR-92b-3p expression are shown in fig. 6L (open arrows). The scale bars for A, E & I are 50 μm, for B, C, D, F, G & H are 10 μm, for J, K & L are 5 μm.

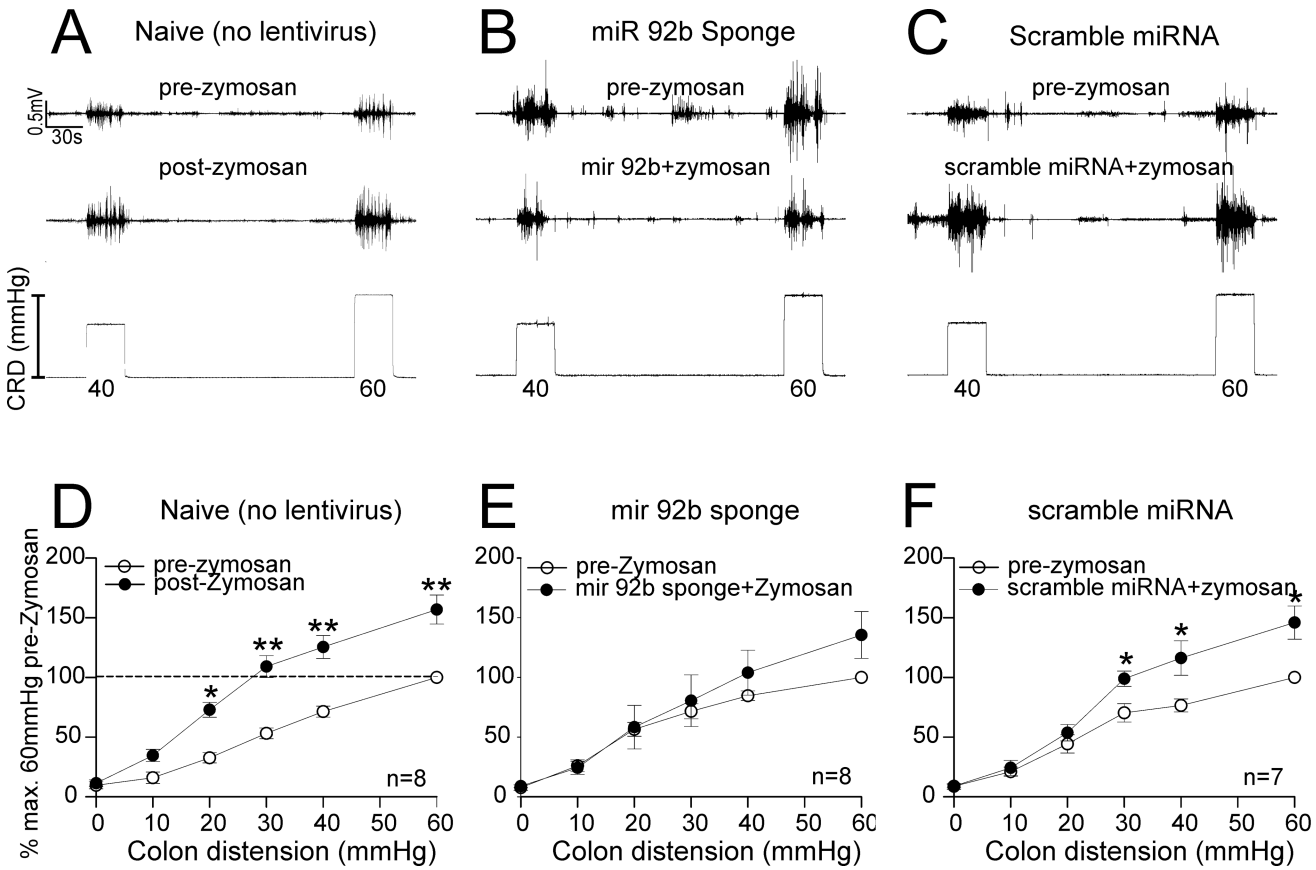

Figure 7.

Effect of preemptive lentiviral miR-92b-3p sponge and scramble control administration on the development of cystitis-induced visceral hyperalgesia (measured by recording the VMR to CRD in rats (n = 7–8/ group). The schematic presentation of the treatment protocols is shown in fig. 1B. Representative EMG tracing to 40–60 mmHg of graded CRD of (A) pre- and post-zymosan in naïve rats, (B) pre- and post-zymosan in rats preemptively treated with lentiviral sponge miR 92b-3p two weeks before zymosan exposures and, (C) pre- and post-zymosan in rats preemptively treated with scramble control two weeks before zymosan exposures. VMR is represented as percentage normalized EMG response to 60 mmHg CRD of pre-treatment baseline. (D) Three days of intravesicle zymosan produced a significant (* $p<0.05$, ** $p<0.01$ vs pre-zymosan) increase in VMR to CRD in adult rats, (E) preemptive lentiviral sponge miR-92b-3p administration attenuates the increase in VMR to CRD seen with only zymosan treatment, (F) preemptive lentiviral scramble control administration demonstrates comparable response (*$p<0.05$ *vs* pre zymosan) as seen with only zymosan treatment.

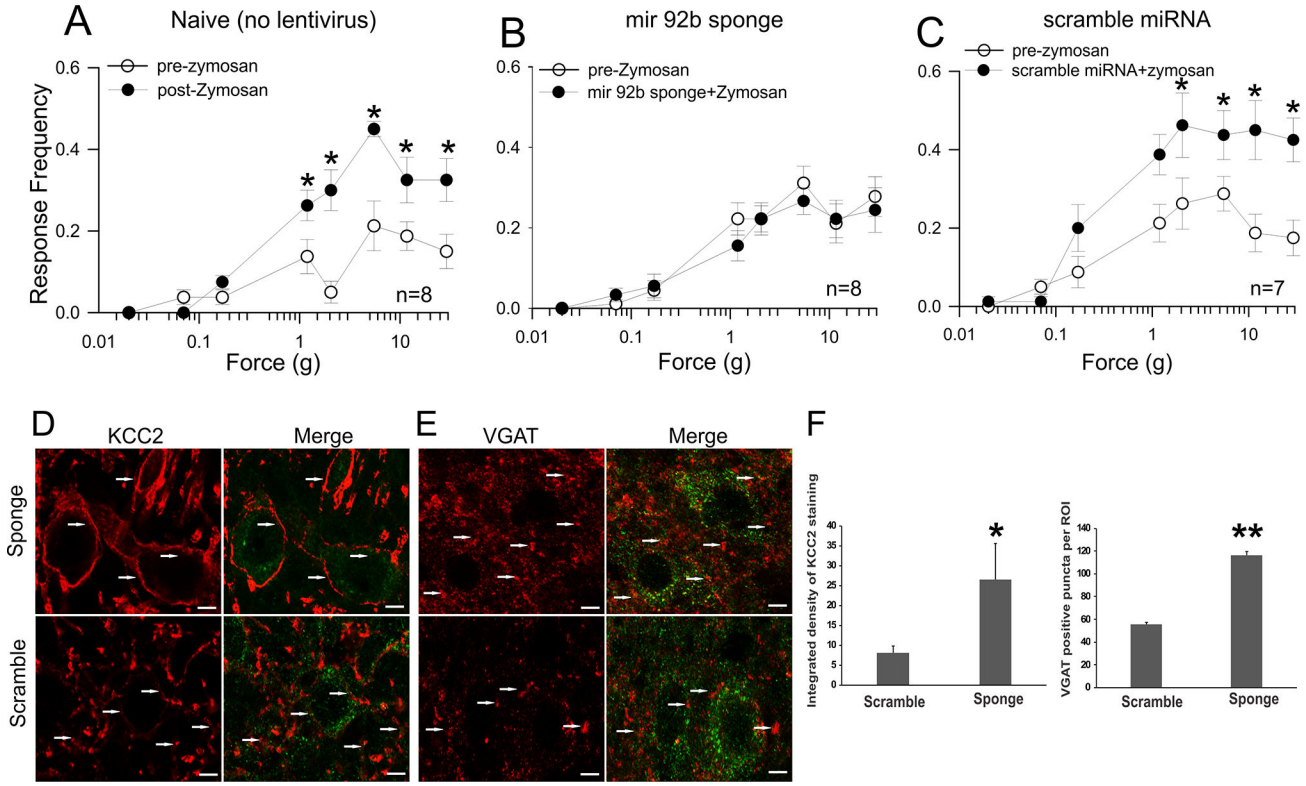

Figure 8.

Effect of preemptive lentiviral sponge miR-92b-3p or scramble control administration on referred hyperalgesia withdrawal frequencies in adult zymosan-treated rats (n = 7–8/group). The schematic presentation of the treatment protocols is shown in fig. 1B. Lentiviral miR-92b-3p sponge induces upregulation of KCC2 and VGAT proteins in dorsal horn of spinal cord (L6-S1) compared with lentiviral scramble control. (A) There is a significant increase in withdrawal response frequencies following 3 days of intravesicle zymosan (*p<0.05 vs pre-zymosan). (B) Preemptive lentiviral sponge miR-92b-3p administration could attenuate the increase in withdrawal response frequencies receiving three days of zymosan treatment. (C) Preemptive lentiviral scramble control administration failed to attenuate the withdrawal response frequencies following intravesicle zymosan treatment (*p<0.05 vs pre-zymosan) which is comparable to the responses of rats in with only intravesicle zymosan exposures. (D) The KCC2 expression pattern in GFP-positive spinal dorsal neurons from rats receiving intrathecal injection of miR-92b sponge and scramble controls (arrows). (E) The VGAT immunostaining of spinal cord (L6-S1) with intrathecal injection of lentiviral miR-92b-3p sponge and scramble control(arrows). (F) The intensity of KCC2 membrane staining in GFP expressed neurons demonstrates significant in lentiviral sponge-treated rats (*p<0.01 vs scramble). The VGAT positive puncta around GFP positive neurons as selected using fixed ROIs also demonstrates significant increase in lentiviral sponge-treated rats (**p<0.001 vs scramble). The scale bar is 5μm.